Supporting Information

Molecular Dynamics Study of Catalytic H_2/O_2 Recombination on Pd, Pt, Cu, Ag, and Au Nanoclusters using Universal Neural Network Potential

Yusuke Tateishi,[a,b] Louise M. Botha,[b] Alina E. Kozhukhova,[b] Manabu Sugimoto,[a,c*] Ken-ichi Aika,[d] and Dmitri G. Bessarabov[b*]

[a] *Faculty of Advanced Science and Technology, Kumamoto University, 2-39-1 Kurokami, Chuo-ku, Kumamoto 860-8555, Japan.*

[b] *HySA Infrastructure, North-west University,11 Hoffman Street, Potchefstroom, 2531, South Africa.*

[c] *Department of Pharmaceutical Sciences, Daiichi University of Pharmacy, 22-1 Tamagawa-machi, Minami-ku, Fukuoka 815-8511, Japan.*

[d] *National Institute of Technology (KOSEN), Numazu College, 3600 Ooka, Numazu, Shizuoka 410-8501, Japan.*

To whom all correspondence should be addressed:
(MS) m-sugimoto@daiichi-cps.ac.jp, (DGB) Dmitri.Bessarabov@nwu.ac.za

This document provides detailed computational methods, additional computational data, and supporting figures that complement the main manuscript.

Table of contents

Detailed Computational Methods

1. Structure Modelling

The nanoclusters were obtained from the Atomic Simulation Environment (ASE) software package.[1] Each nanocluster has an icosahedral structure with five atoms along each edge, consisting of 309 atoms, of which 162 are surface atoms, and a diameter of approximately 1 nm. Geometric optimizations were performed using UNNP implemented in the Matlantis software package. The optimization process employed the limited-memory Broyden-Fletcher-Gold-Shanno (LBFGS) algorithm provided in ASE.[1] Structural convergence was defined by a maximum force criterion of 0.001 eV/Å. When f_{max}< 0.001 eV/Å, the forces acting on the atoms become negligibly small, indicating that the system has reached an energetically stable state.

To simulate the catalytic H_2/O_2 recombination on these nanoclusters, each nanocluster was embedded in a 50 Å cubic unit cell surrounded by 117 H_2 and 58 O_2 molecules, as shown in Fig. 1. The number of O_2 and H_2 molecules was chosen to achieve an equivalent pressure of 100 bar for an ideal gas. The Pt nanocluster was embedded into the simulation cell by removing gas molecules within the embedded region, without altering the overall system pressure (Fig. S1). Using this approach, we we simulated the catalytic performance of the nanoclusters in an H_2/O_2 environment.

2. Molecular Dynamics Simulation

MD simulations were performed using ASE through the Matlantis software interface. The atomic forces (or potential energy) required for the MD calculations were determined using the UNNP with the same settings described mentioned in the previous section. The simulations were performed under the NVT ensemble using the Nosé-Hoover thermostat,[2,3] with a thermostat time constant ($\boldsymbol{\tau}$) of 10 femtoseconds (fs). The temperature was fixed at 500 K, and the volume was fixed at 125,000 Å^3. Each simulation was run for 200 picoseconds (ps) with a timestep of 1 fs. To ensure statistical reliability, three independent simulations were carried out with randomly assigned initial velocities.

The initial pressure of the system was approximately 100 bar, consisting of 117 H_2 and 58 O_2 molecules. It should be noted that the pressure decreased slightly during the simulations due to absorption and reaction processes. These simulation conditions were selected to promote reactions and efficiently evaluate catalytic performance, thereby mitigating the limitations associated with low adsorbent concentrations that typically slows H_2/O_2 adsorption and recombination reactions.

3. DFT calculation

The parameters used for the DFT calculations were consistent with those applied for the UNNP simulations in the Matlantis software. Using DFT, the binding energies of hydrogen and oxygen on the metal surfaces were investigated. Spin-polarized plane-wave DFT calculations were performed with the Vienna Ab Initio Simulation Package (VASP),[4] version 5.4.4. The Perdew–Burke–Ernzerhof (PBE)[5] functional with generalized gradient

approximation (GGA)[5] and the Projector Augmented Wave (PAW) method[6] were employed. The kinetic cut-off was set to 520 eV for the plane-wave basis set of the Kohn–Sham valence states, which was sufficient to avoid Pulay stress. The self-consistent field (SCF) convergence criteria was set to 10^{-6} eV, and the structural optimization was considered converged when the residual atomic forces were less than 0.001 eV/Å. Electronic partial occupancies were determined using Gaussian smearing with a width of 0.2 eV for all calculations.

The D3-BJ dispersion correction with the Becke-Johnson damping function[7] was applied to account for van der Waals interactions in the adsorption systems. The Hubbard U correction was used to describe localized electrons in the d-electrons in transition metals. Following the UNNP parameterization in Matlantis, the U value for the d-orbitals was set to 0 eV for Pt, Pd, Au, and Ag, and 4.0 eV for Cu. For oxygen, a correction value of 0.60 eV was applied to the p-orbitals.

The next section provides additional explanations and context for the supplementary figures presented in this document. These notes clarify methods, parameters, or specific observations related to each figure.

Commented [LB1]: I think we should add some introduction paragraph to the next part. To keep it consistent with your previous sections (Detailed computational methods).

Supplementary Figure Notes

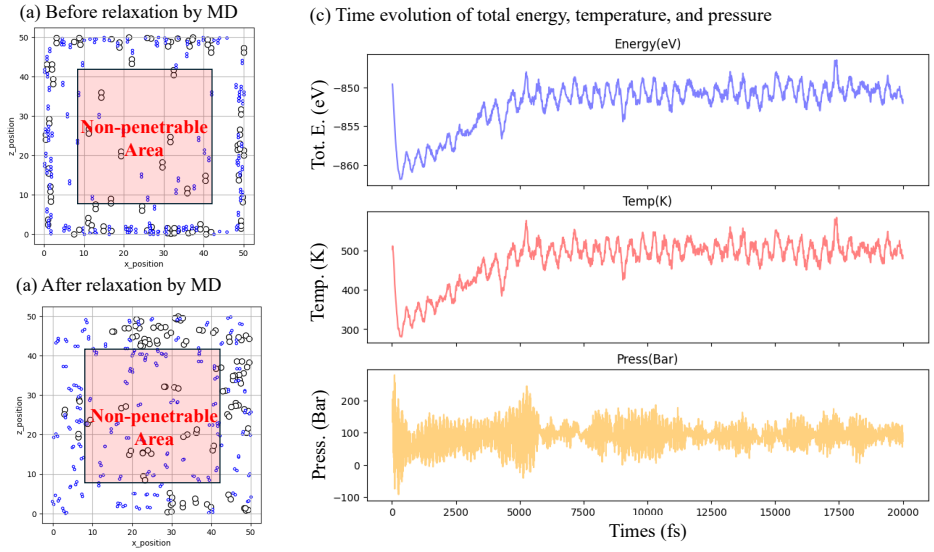

Fig. S1 Preparation and equilibration of the H_2/O_2 gas mixture.

In Fig. S1(a): the initial configuration before molecular dynamics (MD) relaxation is shown. Blue and grey dots represent individual H_2 and O_2 molecules, respectively, randomly packed in a 50 Å cubic cell. The central region (shaded red) defines a non-penetrable cube approximately 30 Å wide.Fig. S2(b): The configuration after a 20 ps NVT run, showing redistribution of the gas molecules outside the non-penetrable region. The molecules visualized inside the cube are those located on the front or back sides of the simulation cell. A Morse wall (fix wall/region) applied to the red region repels any atom attempting to enter, maintaining an empty space for subsequent nanocluster insertion without atomic overlap.

Fig. S3(c): Time evolution of total energy, temperature, and pressure during the same simulation (timestep:1 fs, 500 K, Nosé–Hoover thermostat, Matlantis PFP "CRYSTAL_PLUS_D3" potential ver 6.0.0). The system reached a quasi-steady state at 500 ± 25 K and 80-90 ± 30 bar, with total energy fluctuations within ±3 eV, indicating adequate equilibration and gas-phase dispersion outside the non-penetrable region. The pressure (< 100 bar) arises because the nanocluster volume was subtracted as excluded volume, assuming the nanocluster would be inserted, and the gas-phase mole number was calculated based on the effective volume.

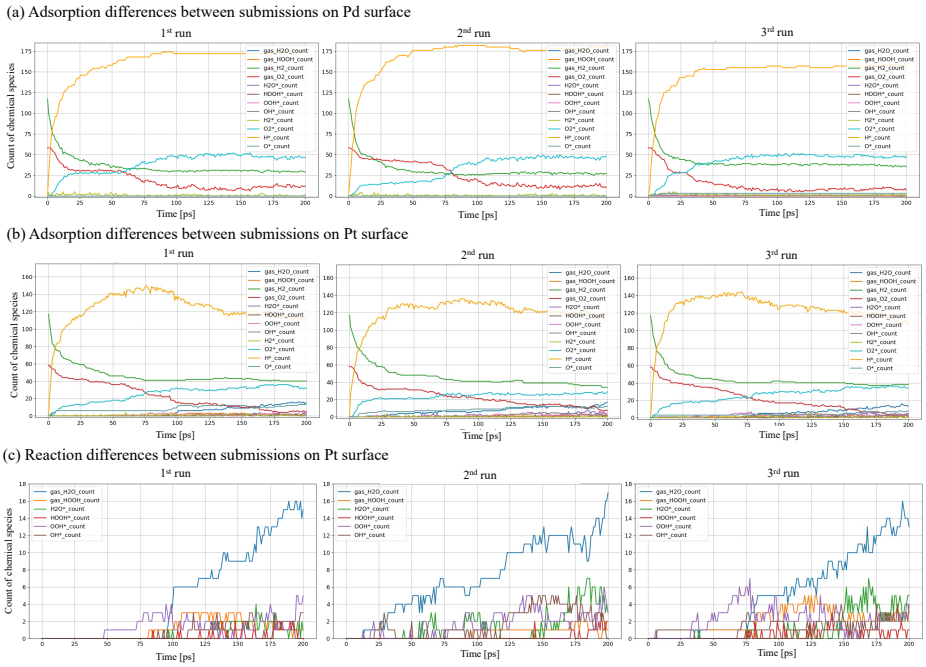

Fig. S2 Comparison of other runs of MD at 500K for Pd and Pt nanocluster. 1st run is the simulation described in the main text. The 2nd run and the 3rd run were additionally executed by changing the initial velocity distribution generated by the random number generator.

In Fig. S2(a), although slight differences are observed in adsorption rates and quantities, the overall reaction behavior of Pd in the H_2/O_2 gas mixture remains consistent, demonstrating the reproducibility of the simulation.

As shown in Fig. S2(b), variations in the adsorption amounts are evident among the three simulation runs. In the second run, O_2 adsorption appears to be lower than in the other runs. Fig. S2(c) illustrates the formation of reaction intermediates and products. In the first and third runs, H_2O formation occurs following OOH* formation, as indicated by the purple lines. On the other hand, in the second run, OOH* and OH* form almost simultaneously prior to H_2O formation, resulting in fewer HOOH* and HOOH species compared with other runs. In any case, OOH* consistently plays a key role in the H_2/O_2 recombination reaction on the Pt surface.

For Cu, Ag, and Au, minor quantitative differences in adsorption amounts were also observed, but the overall H_2/O_2 recombination behavior remained essentially the same as that observed for Pd.

(a) Temperature dependence in adsorption on the Pd surface

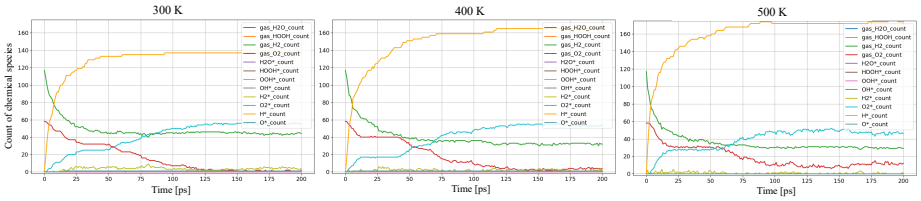

(b) Temperature dependence in adsorption on the Pt surface

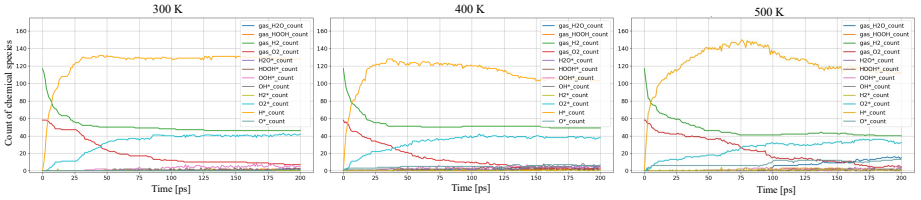

(c) Temperature dependence in reaction on the Pt surface

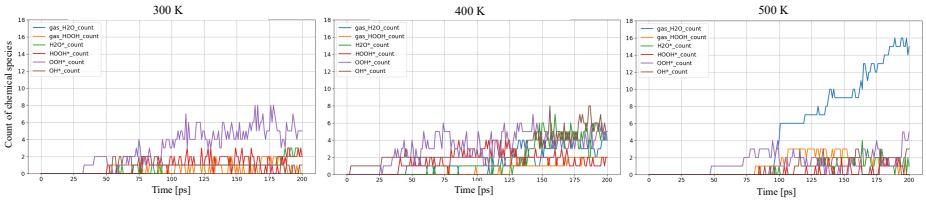

(d) Temperature dependence in adsorption on the Cu surface

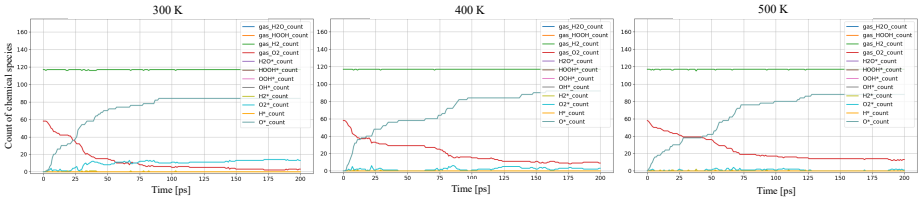

Continued

Continued

(e) Temperature dependence in adsorption on the Ag surface

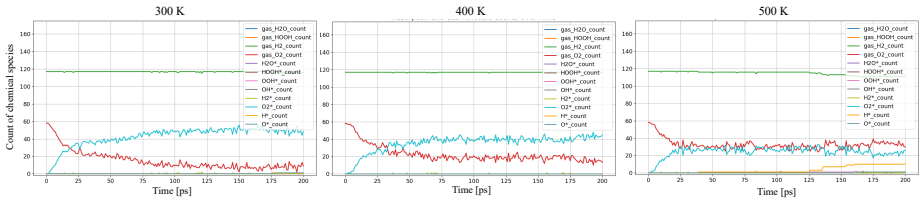

(f) Temperature dependence in adsorption on the Au surface

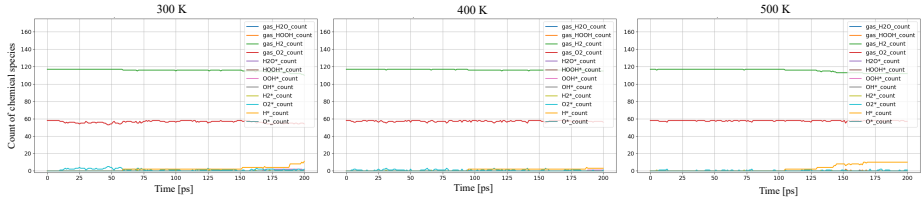

Fig. S3 Performance differences between 300K, 400K, and 500K. The amounts of H_2 and O_2 gas in a simulation system remain consistent at these temperatures.

Fig. S3(a): On the Pd surface, the number of the gas-phase molecules decreased while the amount of H adsorption increased with increasing temperature.

Fig. S3(b): A similar trend was observed on the Pt surface, where the number of the gas-phase molecules decreased andH adsorption increased as temperature rose. O_2 molecules in the gas-phase were more readily adsorbed at 300 K and 400 K. Correspondingly, O_2 adsorption decreased with further increases in temperature. Regarding the reaction process (Fig. S3(c)), on the Pt surface at 300 K, the formation of OOH* and OH* occured. However, no free H_2O was produced in the in the gas-phase. At 400 K, the formation of H_2O*, HOOH*, H_2O, and HOOH was observed. Notably, at 500 K, the number of free H_2O molecules increased, suggesting that the reaction is thermally accelerated.

Fig. S3(d): On the Cu surface, the amount of oxygen adsorbed decreased slightly with increasing temperature, although the temperature dependence was relatively weak.

Fig. S3(e): On the Ag surface, stronger O_2 adsorption was observed at lower temperatures, which may be due to thermal motion of the Ag atoms at higher temperatures.

Fig. S3(f): On the Au surface, temperature variations did not significantly affect the adsorption behavior.

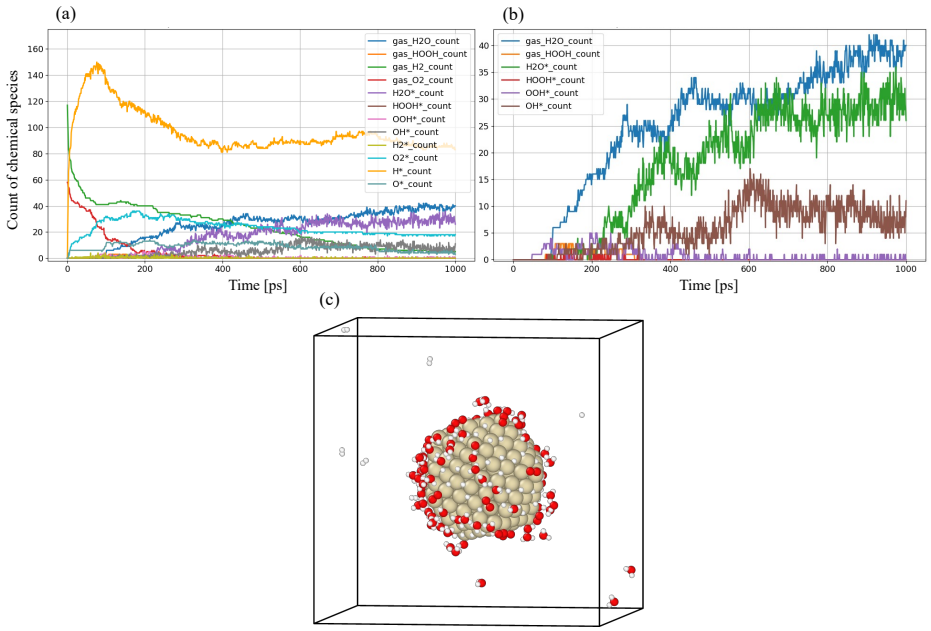

Fig. S4 Time evolution of 1000 ps simulation. (a) shows an overview of the reaction, including reactants (gases). (b) shows the selectivity of the reaction, specifying intermediates and products in more detail. (c) shows simulated structure of Pt nanocluster with H_2O*, OH*, O_2*, etc.

As shown in Fig. S4(a), the number of gas-phase O_2 decreases and was depleted around 200 ps. The number of H_2 molecules steadily decreases until 1000 ps, while the number of adsorbed H* atoms reached a plateau at approximately 100 ps. Thereafter, it gradually declined along with the production of intermediates and products.

In Fig. S3(b), the number of H_2O and H_2O* species increases steadily, confirming the high catalytic activity of the system. In contrast, examination of the intermediates (OH*, OOH*) reveals that the number of OOH* — the source of H_2O* and OH* — is lower than that of OH* after 200 ps. This decrease can be attributed to the depletion of O_2, which is the source of OOH*. The occasionally generated OOH* during 200-1000 ps quickly disappear, suggesting its high reactivity (instability). The amount of OH* remains nearly constant (or slightly decreases), indicating that OH* functions as a key intermediate in water formation. This step appears to be the rate-determining process of the reaction.

As shown in Fig. S4(c), a substantial amount of H_2O and H_2O* is observed on the surface. Numerous H_2O molecules exist loosely bound to the surface—likely through hydrogen bonding rather than direct interaction with the metal atoms. In this analysis, such species were counted as H_2O rather than H_2O*. The accumulation of H_2O on the surface suggestspossible catalyst poisoning.

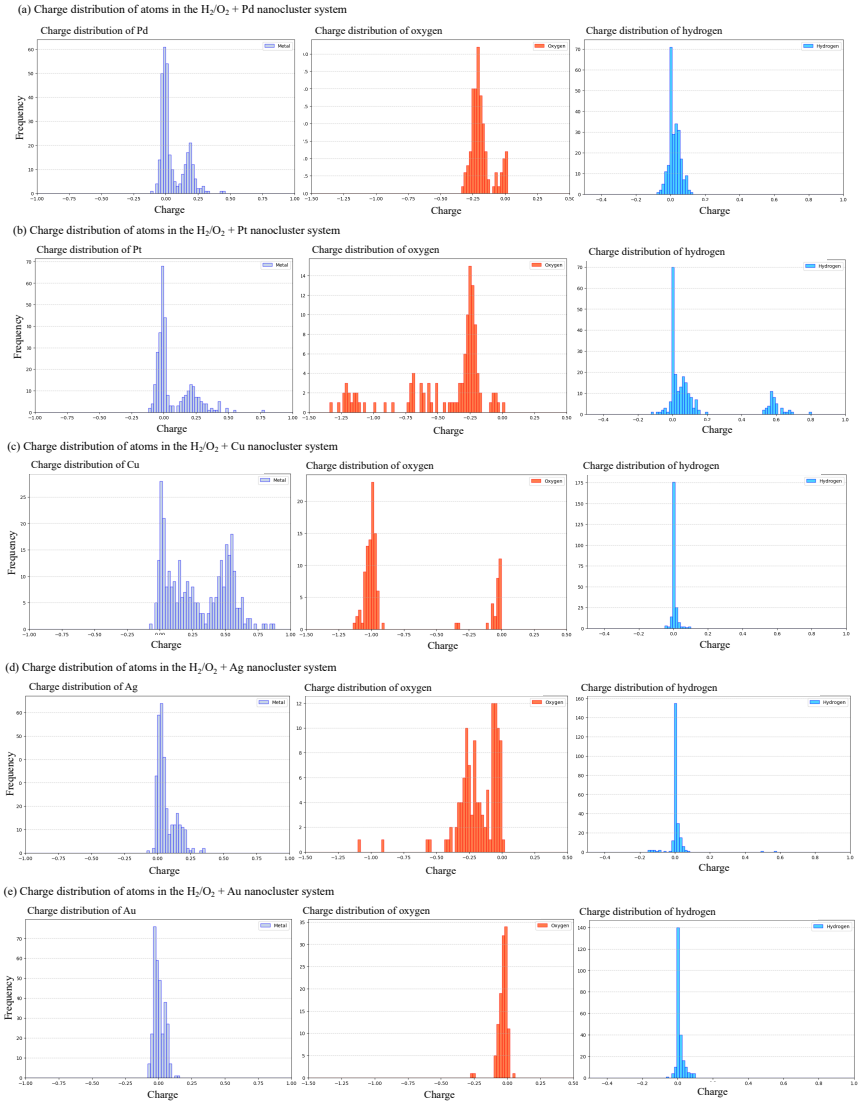

Fig. S5 Charge distribution of atoms in the system: H_2/O_2 + metal nanoclusters after simulation (1st run). (a)-(e) shows the charge distribution of oxygen, hydrogen, and metals, regarding Pd, Pt, Cu, Ag, and Au, respectively.

As shown in Fig. S5(a), several $Pd^{\delta+}$ species are present due to O_2 and H adsorption. The adsorbed O_2 or O atoms are charged δ－as a result of surface oxidization, while H atoms can carry an almost neutral or slightly δ+ charge, consistent with H^+ adsorption on the Pd surface.
In Fig. S5(b), several $Pt^{\delta+}$ species appear due to O_2 and H adsorption. Various positively charged O_2 or O species are observed, likely corresponding to the formation of products and intermediates. On the other hand, H atoms are charged δ+, with a few showing up to 0.6+, consistent with H^+ on the Pd surface. Most products (H_2O, HOOH) and intermediates (OH*, OOH*) exhibit hydrogen charges in the range of +0.5 to +0.65.
In Fig. S5(c), approximately half of the Cu atoms are charged δ+ (around +0.5) due to O adsorption. Nearly all oxygen atoms exhibit a charge of about +1, suggesting the formation of Cu-O-Cu species on the surface. On the other hand, H atoms are nearly neutral, indicating less interaction with the Cu surface.
In Fig. S5(d), several $Ag^{\delta+}$ species appear as a result of O_2 adsorption, with O_2 or O atoms showing positive charges. In contrast, H atoms remain mostly neutrally charged, again indicating minimal interaction on the Ag surface.
Fig.S5(e) shows almost no changes in charge distribution, indicating that Au is inert toward both oxygen and hydrogen.

These observed atomic charge distributions are consistent with the well-known characteristics of these metals, further justifying the use of UNNP in the present study.

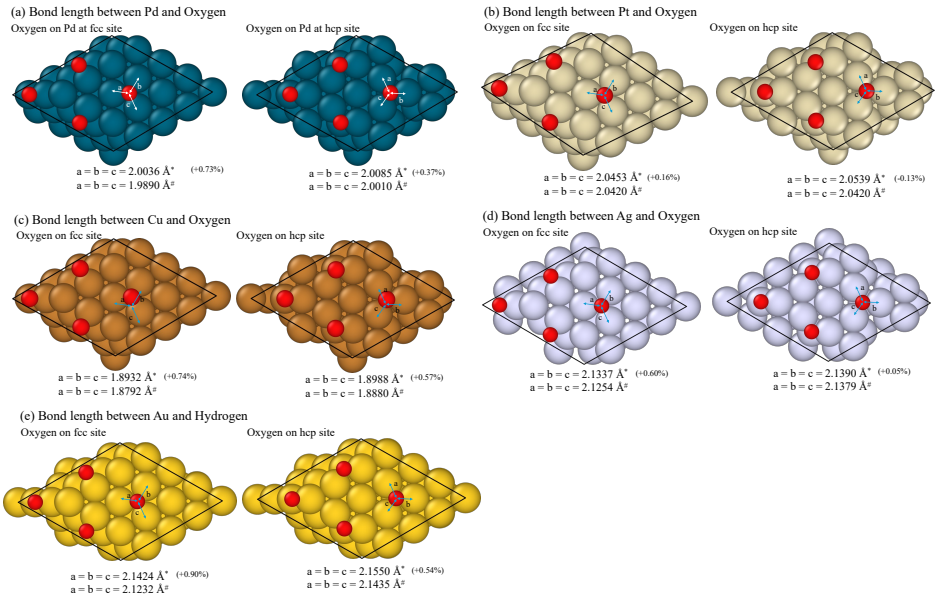

Fig. S6 The bond length between the metal surfaces (slab) and oxygen. The panels (a)-(e) show the surfaces of the slab models for the metals (Pd, Pt, Cu, Ag, and Au) absorbing oxygen atoms shown as small red balls. The structure is expanded to show, while the actual structure is a 2x2 surface with four layers.
* Calculated length by UNNP; # Calculated length by DFT(GGA-PBE) using VASP.

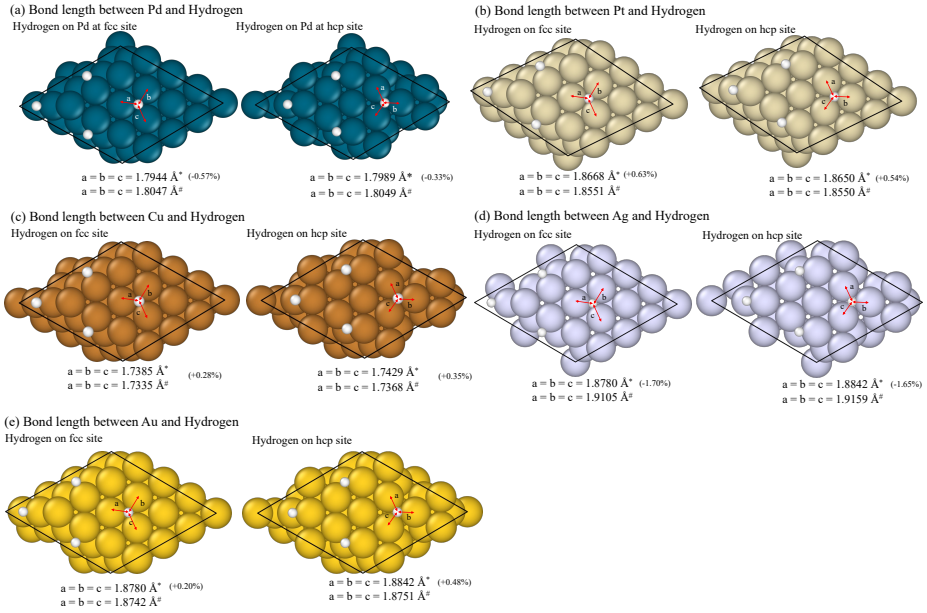

Fig. S7 The bond length between the metal surfaces (slab) and hydrogen. The panels (a)-(e) shows the surfaces of the slab models for metals (Pd, Pt, Cu, Ag, and Au) absorbing hydrogen atoms shown as small red balls. The structure is expanded to show, while the actual structure is a 2x2 surface with four layers.
* Calculated length by UNNP, # Calculated length by DFT(GGA-PBE) using VASP.

As shown in Fig. S5 and Fig. S6, the error between UNNP and DFT was generally less than 1%. Although the Ag-H bond distances were calculated with the errors of -1.65 and -1.70 %, the differences between UNNP and DFT are essentially small.

Tabel S1 Calculated UNNP binding energies (in eV unit) for Pt, Pd, Cu, Ag, and Au, and their comparisons with the DFT(GGA-PBE), DFT (PW91|RPBE), and experimental studies.

	Site	Pd	Pt	Cu	Ag	Au
O	fcc	−4.28* −4.16[#] −3.79 | −3.20 [a]	−3.93* −3.81[#] −3.87 | −3.27 [b]	−4.65* −4.62[#] −4.31 | −3.71 [d]	−3.58* −3.56[#] −3.29 | −2.75 [f]	−2.64* −2.68[#] −2.77 | −2.19 [h]
	hcp	−4.22* −3.94[#] −3.61 | −3.03 [a]	−3.81* −3.43[#] −3.43 | −2.86 [b]	−4.59* −4.50[#] −4.19 | −3.61 [d]	−3.53* −3.46[#] −3.17 | −2.64 [f]	−2.55* −2.51[#] −2.53 |−1.97 [h]
	Exptl.	n.d.	−3.70 [c]	−4.60 [e]	−3.44 [g]	−2.43 [i]
H	fcc	−2.90* −2.85[#] −2.88 | −2.69[a] −2.88 | −2.68 [j]	−2.84* −2.67[#] −2.74 | −2.57[b] −2.72 | −2.55 [j]	−2.54* −2.50[#] −2.45 | −2.27[d] −2.39 | −2.23 [j]	−2.18* −2.20[#] −2.10 | −1.91[f] −2.08 | −1.92 [j]	−2.08* −2.11[#] −2.18 | −2.00[h] −2.22 | −2.07 [j]
	hcp	−2.90* −2.78[#] −2.84 | −2.66[a] −2.84 | −2.65 [j]	−2.85* −2.64[#] −2.71 | −2.55[b] −2.68 | −2.50 [j]	−2.52* −2.50[#] −2.44 | −2.27[d] −2.38 | −2.21 [j]	−2.16* −2.19[#] −2.07 | −1.89[f] −2.06 | −1.90 [j]	−2.05* −2.09[#] −2.14 | −1.96[h] −2.17 | −2.02 [j]
	Exptl.	−2.69 [m]	−2.78 [k]	−2.43 [l]	−1.83 [to] −2.00 [n]	n.d.

* This study (UNNP calculation on nanocluster)
# This study (DFT calculation using 2x2 (111), four-layer slabs with GGA-PBE)
[a] Ref. 8, [b] Ref. 9, [c] Ref. 10, [d] Ref. 11, [e] Ref. 12, [f] Ref. 13, [g] Ref. 14, [h] Ref. 15, [i] Ref. 16, [j] Ref. 17, [k] Ref. 18, [l] Ref. 11, [n] Ref. 19, [m] Ref. 20

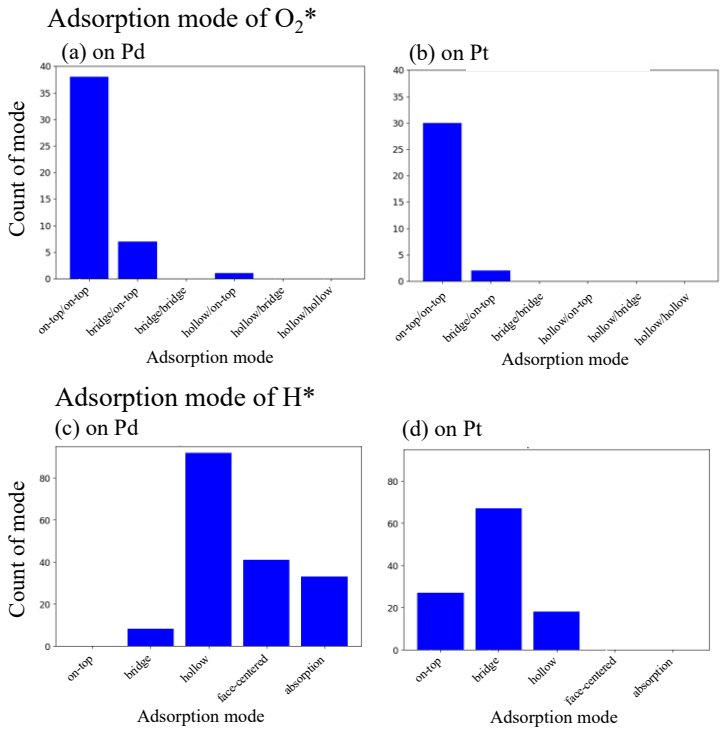

Fig. S8 Site distributions of adsorbed O_2* and H* on Pd and Pt nanoclusters.

In Fig S8(a,b): for both Pd and Pt, the molecular precursor O_2* predominantly occupies the on-top/on-top (1 + 1-fold) configuration, indicating that each O atom prefers to bind to a single surface metal atom. In Fig S8(c): On Pd, dissociated H* atoms are mainly found at hollow (3-fold) sites and other high-coordination environments labelled as face-centred or absorption (subsurface uptake), reflecting Pd's propensity to accommodate subsurface/ensemble hydrogen. In Fig S8(d): Conversely, on Pt, H* populated lower-coordination on-top and bridge (1- or 2-fold) sites, with a smaller fraction at hollow sites. Because both O_2* and H* favor on-top sites on Pt, site competition is likely to occur, indicating selectivity. Whereas, on Pd, the preferred sites were distinct, so that competitive adsorption cannot be occurred.

Mode names were assigned solely on the number of metal atoms within the bonding-cutoff distance of each adsorbate atom: thus, "face-centred" and "absorption" denote highly coordinated or subsurface positions rather than crystallographically strict definitions.

References

1. A. H. Larsen, J. J. Mortensen, J. Blomqvist, I. E. Castelli, R. Christensen, M. Dułak, J. Friis, M. N. Groves, B. Hammer, C. Hargus, E. D. Hermes, P. C. Jennings, P. Bjerre Jensen, J. Kermode, J. R. Kitchin, E. Leonhard Kolsbjerg, J. Kubal, K. Kaasbjerg, S. Lysgaard, J. Bergmann Maronsson, T. Maxson, T. Olsen, L. Pastewka, A. Peterson, C. Rostgaard, J. Schiøtz, O. Schütt, M. Strange, K. S. Thygesen, T. Vegge, L. Vilhelmsen, M. Walter, Z. Zeng and K. W. Jacobsen, The atomic simulation environment - A Python library for working with atoms, *J. Phys.: Cond. Mat.*, 2017, **29**(27), 273002.
2. S. Nosé, A unified formulation of the constant temperature molecular dynamics methods, *J. Chem. Phys.*, 1984, **81**(1), 511–519.
3. W. G. Hoover, Canonical dynamics: Equilibrium phase-space distributions, *Phys. Rev. A*, 1985, **31**, 1965-1967.
4. G. Kresse and J. Furthmiiller, Efficiency of ab-initio total energy calculations for metals and semiconductors using a plane-wave basis set, *Comput. Mat. Sci.*, 1996, **6**(1), 15-50.
5. J. P. Perdew, K. Burke and M. Ernzerhof, Generalized Gradient Approximation Made Simple, *Phys. Rev. Lett.*, 1996, **77**, 3865-3868.
6. P. E. Blochl, Projector augmented-wave method, *Phys. Rev. B*, 1994, **50**, 17953-17959.
7. A. D. Becke, E. R. Johnson, Exchange-hole dipole moment and the dispersion interaction, *J. Chem. Phys.*, 2005, **122**(15), 154104.
8. J. A. Herron, S. Tonelli and M. Mavrikakis, Atomic and molecular adsorption on Pd(111), *Surf. Sci.*, 2012, **606**, 1670–1679.
9. D. C. Ford, Y. Xu and M. Mavrikakis, Atomic and molecular adsorption on Pt(111), *Surf. Sci.*, 2005, **587**, 159–174.
10. J. L. Gland, B. A. Sexton and G. B. Fisher, Oxygen interactions with the Pt(111) surface, *Surf. Sci.*, 1980, **95**(2–3), 587-602.
11. L. Xu, J. Lin, Y. Bai and M. Mavrikakis, Atomic and Molecular Adsorption on Cu(111), *Top Catal.*, 2018, 61, 736–750.
12. R. Naumann d'Alnoncourt, B. Graf, X. Xia, and M. Muhler, The back-titration of chemisorbed atomic oxygen on copper by carbon monoxide investigated by microcalorimetry and transient kinetics, *J. Therm. Anal. Calorim*., 2008, **91**, 173–179.
13. B. W. J. Chen, D. Kirvassilis, Y. Bai and M. Mavrikakis, Atomic and Molecular Adsorption on Ag(111), *J. Phys. Chem. C*, 2019, **123**, 7551–7566.
14. T. Campbell, Atomic and molecular oxygen adsorption on Ag(111), *Surf. Sci.*, 1985, **157**, 43-60.
15. Y. Santiago-Rodríguez, J. A. Herron, M. C. Curet-Arana and M. Mavrikakis, Atomic and molecular adsorption on Au(111), *Surf. Sci.*, 2014, **627**, 57–69.
16. N. Saliba, D. H. Parker and B. E. Koel, Adsorption of oxygen on Au(111) by exposure to ozone, *Surf. Sci.*, 1998, **410**, 270–282.
17. J. Greeley and M. Mavrikakis, Surface and Subsurface Hydrogen: Adsorption Properties on Transition Metals and Near-Surface Alloys, *J. Phys. Chem. B*, 2005, **109**, 3460–3471.

18. G. Mechtersheimer and G. Comsa, The interaction of hydrogen with platinum(s)−9(111) × (111) studied with helium beam diffraction, *Surf. Sci.*, 1981, **111**, 519-544.
19. G. Lee, P. T. Sprunger, M. Okada, D. B. Poker, D. M. Zehner and E. W. Plummer, Chemisorption of hydrogen on the Ag(111) surface, *J. Vac. Sci. Technol. A*, 1994, **12**, 2119–2123.
20. K. Christmann, Interaction of hydrogen with solid surfaces, *Surf. Sci. Rep.*, 1988, **9**, 1–163.